# An *ab initio* study of self-trapped excitons in $\alpha$-quartz

Renée M. Van Ginhoven and Hannes Jónsson[a)]
*Department of Chemistry, University of Washington, Seattle, Washington 98195-1700*

Kirk A. Peterson, Michel Dupuis, and L. René Corrales[b)]
*Pacific Northwest National Laboratory, Richland, Washington 99352-0999*

(Received 21 November 2002; accepted 15 January 2003)

The structure and properties of self-trapped excitons (STE), were investigated using density functional theory (DFT) and wave function-based [UHF, UMP2, CAS-SCF, and CCSD(T)] electronic structure methods. The DFT results were compared to those obtained using the different wave function-based electronic structure methods that treat the electron correlation and exchange with varying degrees of accuracy. The calculations were carried out on cluster configurations extracted from supercell DFT calculations of the STE in $\alpha$-quartz. Two luminescent STEs were found, as well as a nonradiative state at a crossing of the singlet and triplet surfaces. One of the luminescent STEs is the same as that previously found by Fisher, Hayes, and Stoneham [J. Phys.: Condens. Matter **2**, 6707 (1990)]. It was furthermore determined that the PW91 functional underestimates the energy of the triplet state, and that this error is greater with greater delocalization of the excess spin density of the state. © *2003 American Institute of Physics.*
[DOI: 10.1063/1.1559139]

## I. INTRODUCTION

The interaction of radiation with silica causes electronic excitations that promote an electron from the valence band to the conduction band, leaving a hole in the valence band.[1] In general, electrons are excited to the singlet $S_1$ state and higher from which interstate crossings eventually populate the triplet $T_1$ state.[2] When an excited electron and a hole in the valence band remain bound together by Coulomb interactions they are collectively referred to as an exciton. Of interest in this work are the long-lived triplet excitons that in silica have lifetimes in the range of milliseconds. An exciton can become trapped at a distortion in the lattice and is then referred to as a self-trapped exciton (STE). These STEs recombine to the ground state via a spin-forbidden transition, producing a characteristic luminescence. Previous calculations have shown that excitons can facilitate bond breaking and lower diffusion barriers.[3] Experiments indicate that the production of excitons is correlated with the accumulation of defects. Silica glasses that support excitons under irradiation can develop oxygen bubbles and eventually degrade to sand.[4]

Quartz is the most stable crystalline allotrope of silica at ambient temperature and pressure, and has been studied extensively. When quartz is irradiated at energy greater than 7 eV, it expands and exhibits luminescence with a lifetime in the range of 1 ms at low temperature ($<$180 K).[5] Nonradiative processes also occur that manifest as heating in the sample.[5] If the incident flux exceeds a certain threshold, quartz becomes permanently damaged.[4] When below threshold irradiation is discontinued, the luminescence ceases, and the structure returns to the perfect crystal state.[5] The effects are also temperature dependent. The luminescence associated with self-trapped excitons is quenched at temperatures greater than 180 K.

Experiments have shown that when quartz is subjected to irradiation with a laser pulse of less than 100 fs and carried out below the quenching temperature of the excitons, the luminescence is intense in the range associated with the STE, and no permanent defects are formed. Irradiation at 300 K produces no STE luminescence, but does produce defects in the form of oxygen vacancies that are known as $E'$ centers,[6,7] of which there are many forms. The time scale for trapping excitons is about 150 fs. Experimental results also indicate the presence of a thermally activated nonradiative decay process.[8]

A number of luminescence bands have been observed experimentally in $\alpha$-quartz. There are two broad luminescence bands, one centered at 2.8 eV, and the other at 4.0 eV.[8] Both bands are believed to have multiple contributing sources, some from defects or impurities. On the basis of a number of different experiments and theoretical calculations,[9] one contributor to the broad band centered at 4.0 eV has been identified as an oxygen vacancy.[10]

The second emission band, centered at 2.8 eV, has at least three sources. One of these has been identified as arising from an electron–hole recombination at an aluminum impurity (compensated by alkali metal ions).[11] The major part of the luminescence consists of at least two overlapping bands with peak energies of 2.5 and 2.8 eV.[12,13] The 2.5 eV band is quenched at about 130 K, and is polarized perpendicular to the $c$ axis of the quartz crystal. The 2.8 eV band is quenched beginning at 160 K, has a degree of polarization of about 50 percent parallel to the $c$ axis of the crystal, and has a luminescence lifetime of about 1 ms in the low temperature limit. The excited state leading to the 2.8 eV emission is a triplet state,[14] and has been linked to both a transient volume change (expansion) and transient absorption at 5.5 eV. It is

a)Electronic mail: hannes@u.washington.edu
b)Electronic mail: rene.corrales@pnl.gov

 

well accepted that this band is due to an intrinsic self-trapped exciton (STE).[15] The observed luminescence energy displays variations that depend on the experimental conditions, and the presence of impurities or defects in the sample[16] that contribute to the broadening of the bands.

In this work, we present an overview of previous results for the STE in quartz as well as new calculations. The methodology used in the present calculations is discussed, and results from cluster-based calculations of the STE in $\alpha$-quartz are presented.

### A. Previous theoretical results

#### 1. Review of results using cluster models of the STE in quartz

Previously, Fisher *et al.*[1] predicted the structure of the triplet state STE in quartz using unrestricted Hartree–Fock (UHF) calculations with a minimal basis set on small silica clusters of formula $Si_5O_4$ and $Si_2O_7$. Either three or five atoms in the interior of the cluster were free to move. Use of small clusters in determining structures of the STE involves the neglect of lattice relaxation effects as well as long-range forces. The majority of the motion was confined to a single oxygen atom, which was displaced by 0.98 Å, leading to a broken Si–O bond. The Si–O distance increases to 2.45 Å (as compared to the ground-state equilibrium bond distance of 1.61 Å). The predicted luminescence energy, calculated as the energy difference between the triplet and singlet states for a given geometry, was 1.5–l.9 eV, depending on whether a silicon-centered or oxygen-centered cluster was used. In this work, the STE structure of the type having one broken Si–O bond will be referred to as STE-**A**.

The STE-**A** structure is thought to be a precursor to a structure which results in a nonradiative decay.[17] The proposed structure is an oxygen interstitial–vacancy defect pair.

In a study of optical transitions of quartz clusters containing defects, Pacchioni *et al.*[18] predicted an $S_0$ to $S_1$ transition energy of 8.80 eV, as compared to the estimated experimental value of 8.9 eV for quartz. Those calculations were carried out for perfect quartz clusters using similar basis sets as those in this work, and used multireference-doubles-configuration-interaction (MRDCI).

#### 2. Review of supercell calculations of the STE in quartz

More recently, Song *et al.*[19] performed STE calculations using DFT with the PW91 functional and a plane-wave basis set on a periodic (supercell) configuration of quartz, with 72 atoms in the unit cell. These calculations should be more representative of the bulk state of quartz than small clusters. Details of the calculation are provided in Ref. 19. Table I shows the predicted singlet–triplet splittings.[19] At this level of theory, the perfect crystal is the lowest energy structure in the triplet state. However, displacement of an atom from the crystal position by as little as 0.1 Å allows the system to cross an apparent potential energy barrier and relax to a stable distorted state. Two STE structures were found. The first STE structure has three slightly displaced oxygen atoms, with bonds stretched to 1.76 Å from 1.6 Å, and a silicon atom displaced to be nearly planar with the three oxygen atoms. This structure will be referred to as the oxygen-distorted STE structure, or STE-**B**. The second STE structure has one silicon atom displaced through the plane of three oxygen atoms to a puckered configuration, and a broken silicon–oxygen bond, with a distance of 2.54 Å. This structure will be referred to as the silicon-distorted STE, or Si-dist. When the geometry of the distorted structures was relaxed in the singlet state, the system returned to the perfect crystal geometry, which is consistent with experimental results.

TABLE I. Summary of supercell DFT results using 72 atoms, subject to periodic boundary conditions, as described in Ref. 19. $T_1-S_0$ is also the luminescence energy. $E_{rel}$ is the relaxation energy of the system in the triplet state, i.e., the energy of the given geometry relative to the initial triplet excitation of the perfect crystal. The negative energies reported for $E_{rel}$ indicate that the STE is higher in energy than the initial triplet excitation for the perfect crystal.

| Geometry | $T_1-S_0$ (eV) | $E_{rel}$ |
|---|---|---|
| Perfect crystal | 6.1 | ··· |
| STE-**B** | 3.72 | −0.43 |
| STE-**A** | 2.74 | −0.93 |
| Si-distorted | 0.9 | −0.65 |

The STE-**A** type structure is *not* a stable minimum in the supercell DFT/PW91 calculations,[19] although it can appear to be stable in a cluster calculation using the plane-wave DFT method with a relatively loose energy convergence criterion of 0.05 eV between successive steps. With the same initial atom displacement as used in the periodic system, the resulting geometry is similar to that initially found by Fisher *et al.*, with a slightly shorter Si–O distance of 2.3 Å. When this calculation was repeated, using the same tight, gradient-based convergence criterion as was applied to the supercell systems, this structure was not a minimum on the PW91 energy surface. Forces during the relaxation process in the periodic system are quite small in magnitude in the region around this geometry, of about 0.03 eV/Å. This small magnitude in the force reinforces the need for the relatively tight force convergence criterion of 0.01 eV/Å used throughout this work. There is a plateau in this region of the potential energy surface, but not a minimum. With further relaxation, ultimately a different state was reached. Since a minimum for this type of structure is found readily using other electronic structure methods, such as UHF, the configuration at the point of minimum force was included as a possible STE structure (of type STE-**A**).

Band gaps predicted by DFT can be too small as in, for example, pure silicon where the DFT predicted value is half of the experimental value.[20] In silica, the DFT predicted value of 6.0 eV is two-thirds of the experimentally estimated value of 9 eV. In addition, as also shown in Table I, the STE distorted states are found to be higher in energy than the perfect crystal, which is inconsistent with experimental measurements.

The purpose of the work presented in this paper is to investigate the quality of the DFT results, by performing further calculations at higher levels, and comparing the lu-

minescence energies calculated by different *ab initio* methods. The aim is to determine what level of theory is required to accurately characterize the energetics and structure of the self-trapped exciton in quartz.

## II. THEORETICAL APPROACH

### A. Computational methods

The singlet and triplet state energy of specific fixed structures were calculated by each method described below. Because high-level *ab initio* methods cannot be applied to extended systems using periodic boundary conditions, it is necessary to use clusters to approximate the structures obtained with the periodic DFT calculations of Song *et al.*[19] The *ab initio* methods used in this work were restricted Hartree–Fock (RHF), unrestricted Hartree–Fock (UHF), complete active space self-consistent field (CASSCF), and coupled-cluster, singles and doubles plus perturbative triples [CCSD(T)]. Unrestricted Møller–Plesset perturbation (UMP2) calculations were carried out for some clusters, though they were not sufficiently informative to justify the computational costs for all clusters, especially the larger ones. In order to compare the results of different DFT functionals, DFT calculations were performed using the PW91, and B3LYP functionals. Approximate lifetimes of the STE luminescence were calculated with spin–orbit calculations.

Geometry minimizations were performed on a subset of the clusters used in the single-point calculations to validate the geometry of the STE structures. The geometry minimizations were performed on the triplet state at the UHF level, and with DFT, using the PW91 and B3LYP functionals, as described below. A series of increasingly larger basis sets, 6-31G* to aug-cc-pVTZ, were used for the smallest clusters to test for basis set convergence. HF, UHF, UMP2, and DFT calculations were done with GAUSSIAN 98,[21] CASSCF calculations were performed using HONDO,[22] and CCSD(T) and spin–orbit calculations were carried out using MOLPRO.[23] UHF and B3LYP geometry minimization calculations were carried out with HONDO.

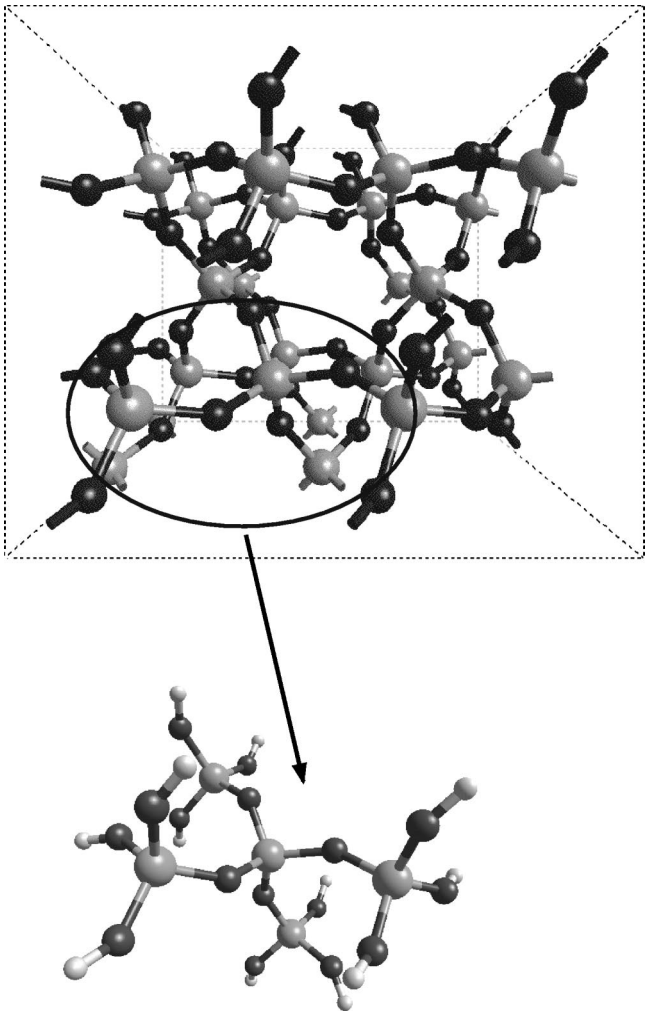

FIG. 1. Selected portions of the 72 atom periodic configuration were extracted as shown. A cluster centered on the region of interest was carved out such that the terminal atoms are oxygen atoms. The cluster was then capped with hydrogen atoms (shown in white) placed in the direction of the next-nearest silicon atoms, at a distance of 0.8 Å. The configuration shown is that of the perfect quartz crystal, with silicon atoms shown in light gray and oxygen atoms in dark gray.

### B. Cluster construction

Three sizes of clusters were used in this work, with formulas $Si_2O_7H_6$, $Si_5O_{16}H_{12}$, and $Si_8O_{25}H_{18}$. Only the smallest clusters are amenable to high-level treatment of electron correlation. These are similar to the oxygen-centered cluster used by Fisher *et al.*[1] Larger clusters are better able to capture the relaxation of the silica network, but are considerably more computationally expensive. Some balance must be found between errors due to the finite size of the cluster, and those errors due to limitations in the accuracy of the method and size of basis set, for which computational feasablity depends on the given cluster size.

Figure 1 illustrates the extraction of a cluster from the original supercell DFT results. The relaxed triplet state of the periodic system was analyzed to determine the location of the STE-induced distortion, and a subset of atoms that contained as much of the distorted region as possible was snipped out of the larger periodic configuration. The clusters were constructed so that the surface atoms were oxygen atoms, with bonds capped by hydrogen atoms. There are no Si–H bonds because the use of Si–H bonds alters the charge and bond characterstics of the Si atoms away from Si–O character.[24] The capping hydrogen atoms were placed at a distance of 0.80 Å away from the oxygen atoms (see below for more details), in the direction where the adjacent silicon atom would be in the supercell configuration. The smaller clusters were relatively straightforward to select for the perfect crystal, and for the silicon-distorted state. There were three candidates for the oxygen-distorted state, since three oxygen atoms were distorted by similar amounts. A preliminary calculation was performed on each possibility, and the cluster in which the hole appeared on the central oxygen was chosen as most representative. It was not possible to extract clusters larger than the $Si_8O_{25}H_{18}$ clusters for any of the STEs without including an unacceptably large amount of the periodic image of the interesting distorted region. Figure 2 shows an example of each of the cluster sizes used for the perfect crystal state.

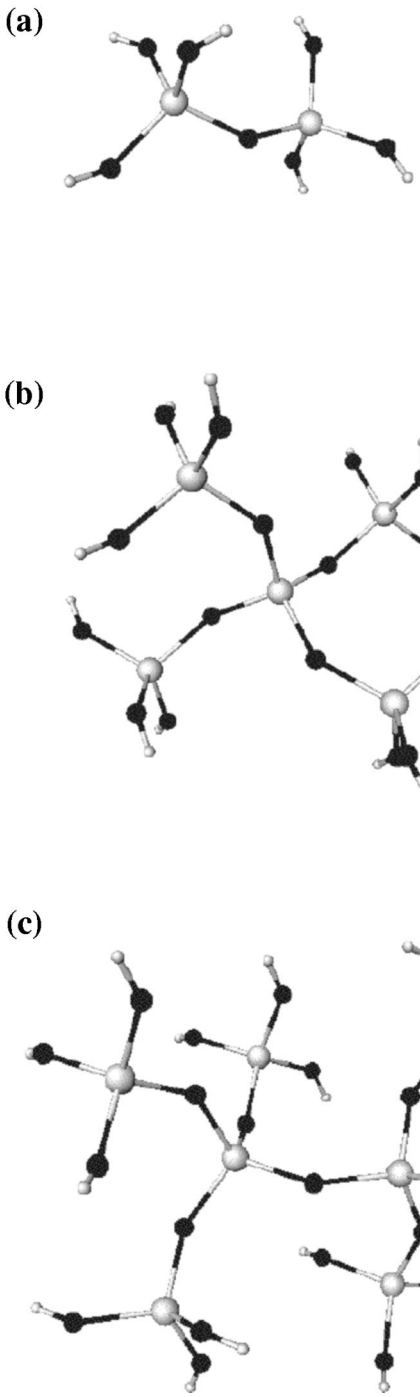


FIG. 2. Illustrations of each of the three cluster sizes used in this work: (a) $Si_2O_7H_6$, (b) $Si_5O_{16}H_{12}$, and (c) $Si_8O_{25}H_{18}$. All the clusters are terminated by oxygen, capped with hydrogen atoms.

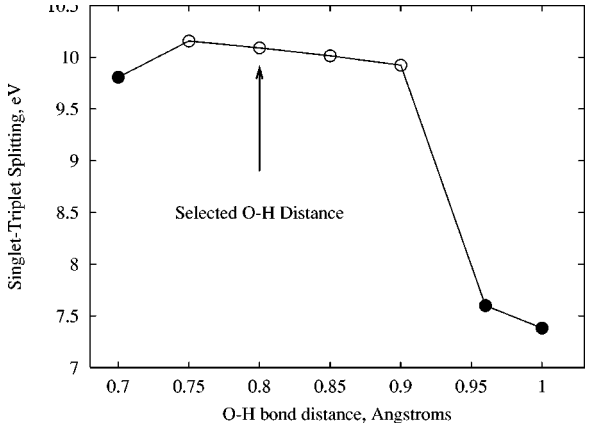


FIG. 3. The singlet–triplet splitting of the perfect crystal cluster changes as the terminating O–H bond length is varied. At bond lengths indicated by filled circles, for both long (0.95 to 1.0 Å) and short (0.7 Å) bonds, the HOMO of the triplet state is located on the O–H bonds. This results in the exciton localizing on the edge of the cluster, on one or more O–H bonds. For intermediate O–H distances, indicated by open circles, the HOMO (and therefore the exciton) is confined to the interior of the cluster. The $S/T$ shown was calculated for the $Si_2O_7H_6$ cluster, at the UHF level with the 6-31G* basis.

Since the intent is to investigate the luminescence energy in the bulk, and to compare these results with a supercell calculation, the clusters were constucted so that their interiors would mimic bulk quartz as much as possible. Previous calculations on silica, and other systems, have used such techniques as embedding the cluster in an array of point charges,[25] or terminating the cluster dangling bonds with pseudoatoms, or hydrogen atoms.[9] In this work, capping with hydrogen atoms was chosen. Previous calculations have placed the capping hydrogen atoms at close to the O–H equilibrium bond length, 0.96–0.98 Å[18,26] and as close as 0.92 Å.[27] However, Mulliken analysis of the triplet state of the $Si_2O_7H_6$ perfect crystal cluster revealed that with the O–H distance set to 0.96 Å, the triplet state excitation involves the surface O–H bonds. The hole is on an edge oxygen atom, and the excited electron is on a hydrogen atom. By varying the oxygen–hydrogen bond length, it is possible to force the excess spin density of the triplet state to be localized in the interior of the cluster, and not spill over onto the hydrogen atoms. As shown in Fig. 3, for O–H bond lengths between 0.90 and 0.75 Å, the singlet–triplet splitting remains at around 10 eV. Analysis of the triplet state at each bond length in this range shows that the hole is on the central oxygen, and the excited electron is on a silicon atom. For O–H bond lengths shorter than 0.75 Å, the hole is on an edge oxygen, the excited electron is on a hydrogen, and the singlet–triplet splitting is generally smaller.

Figure 4 shows the Mulliken charges on the central oxygen and edge oxygen atoms of the singlet state as a function of O–H bond distance. The charges are most nearly the same when the bond length is 0.80 Å. Since all oxygen atoms in a perfect quartz crystal are charged the same, the 0.80 Å bond length is the logical choice to mimic bulk quartz and was therefore chosen for this work. The charge on the central oxygen atom is constant through the entire range of O–H bond lengths used, which confirms that altering the terminal O–H bond lengths does not significantly alter the center of the cluster.

It should be noted that problems caused by the O–H bond length were only an issue with the perfect crystal. If there is a sufficient distortion of one or more Si–O bonds in the interior of the cluster, there is no interference from the O–H bonds. However, to enable consistent comparison of the results for distorted clusters with the perfect crystal state, the same O–H bond was used in all the single-point calculations, and for all the cluster minimizations (described be-

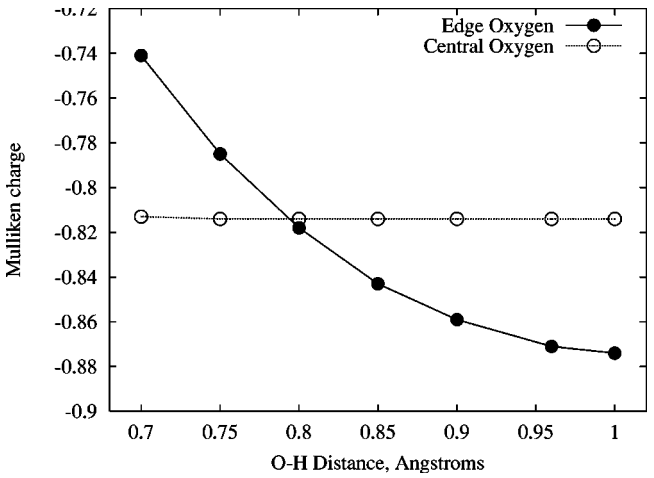


FIG. 4. The charge on the outer oxygen atoms changes as the terminating O–H bond length is varied. As the terminal O–H bonds on the $Si_2O_7H_6$ perfect crystal cluster are shortened, the average Mulliken analysis charge for the edge oxygens (filled circles) becomes less negative, while the charge on the central oxygen (open circles) is unchanged. At an O–H bond distance of 0.8 Å, the charges on the edge and central oxygen atoms are approximately equal.

low), unless indicated otherwise. Singlet–triplet differences were calculated for all three cluster sizes. Spin–orbit coupling calculations were only performed for the smallest size clusters.

To investigate the effect of the cluster environment, as well as the use of different computational schemes, geometry optimizations were performed on a subset of the clusters. The clusters used for the geometry minimizations were all of formula $Si_5O_{16}H_{12}$. In each case, the terminal hydrogen atoms and surface oxygen atoms were frozen, while the interior nine atoms were allowed to move freely. Freezing the exterior atoms provides a simple means of approximating the embedding of a cluster in a bulk system.[28] Clusters with initial geometries corresponding to each of the three distorted structures, STE-**A**, STE-**B**, and Si-dist, were relaxed on the triplet state surface using UHF, and DFT with the PW91 functional and with the B3LYP functional. The basis set used for the geometry optimizations was the 6-31G* basis set.

## III. RESULTS AND DISCUSSION

### A. The effect of basis set and cluster size on the singlet/triplet splitting

Calculations were carried out with increasing cluster size and increasing basis set to determine the basis set size needed to adequately describe the triplet excited state, and the cluster size required to adequately represent a bulk structure. Results are presented separately for each geometry studied.

#### *1. Perfect quartz*

Results for the single-point calculations on the perfect crystal geometry clusters are shown in Table II. The experimental estimate for the $T_1-S_0$ splitting is 8.3 eV.[8] The calculations using DFT are consistently lower than the experimental value, while UHF and UMP2 results are higher. This is consistent with typical underestimation of band gaps in materials as calculated by DFT.

TABLE II. Singlet/triplet splittings for the perfect crystal (quartz) cluster configurations. The singlet/triplet splittings for these clusters is the energy of the initial excitation into the lowest triplet state from the singlet ground state. The *s* is a standard Pople-style *s*-type diffuse function, with a gamma exponent of 0.033 for silicon, and 0.0854 for oxygen. The $s+p$ basis set adds the Pople *p*-type diffuse functions to each heavy atom.

| | Basis set | | | | |
|---|---|---|---|---|---|
| Cluster size | 6-31G* | $+s$ | $+s+p$ | cc-pVTZ | aug-cc-pVTZ |
| $\mathbf{Si_2O_7H_6}$ | | | | | |
| UHF | 10.09 | 9.0 | 8.78 | 9.64 | 8.94 |
| UMP2 | 10.47 | 9.59 | 9.52 | | |
| CCSD(T) | 9.76 | 8.81 | 8.66 | | |
| DFT-PW91 | 7.45 | 6.69 | 6.68 | 7.48 | 6.59 |
| DFT-B3LYP | 8.46 | 7.62 | 7.59 | 8.41 | 7.48 |
| $\mathbf{Si_5O_{16}H_{12}}$ | | | | | |
| UHF | 10.12 | 10.15 | 9.93 | | |
| UMP2 | 10.40 | | | | |
| DFT-PW91 | 7.28 | 6.29 | 6.29 | | |
| DFT-B3LYP | 8.30 | 7.49 | 7.48 | | |
| $\mathbf{Si_8O_{25}H_{18}}$ | | | | | |
| UHF | 10.12 | 10.15 | | | |
| DFT-PW91 | 7.28 | 6.41 | | | |
| DFT-B3LYP | 8.30 | 7.61 | | | |

The results for the different-sized clusters are very similar for the same basis set and method. The addition of diffuse basis functions results in the singlet/triplet splitting being roughly 1 eV smaller. It has previously been shown that diffuse functions are needed to correctly describe excited states in quartz.[18] The use of triple-zeta basis sets does not change the predicted singlet–triplet difference significantly for the DFT calculations. Larger calculations with these larger basis sets were not feasible.

For the DFT-PW91 and DFT-B3LYP calculations, the difference between the triplet and singlet state energy seems to be reasonably converged with the addition of just one *s* diffuse function per heavy atom. The B3LYP calculations give 1.2 eV larger singlet–triplet splitting than PW91 for the larger clusters, and are significantly closer to the experimentally determined band gap of quartz.

Figure 5 shows the excess spin density of the $Si_5O_{15}H_{12}$ cluster representing the perfect crystal. The excess spin is located primarily on the oxygens, and is spread relatively evenly over the entire cluster, indicating that the exciton for this configuration is highly delocalized. In the bulk, the extent of delocalization is expected to be finite, although perhaps larger than the extent of the clusters in these calculations. The excited electron occupies the conduction band and the hole occupies the highest state in the valence band associated with the *p* states of the lone pair orbitals.

#### *2. STE-B*

Figure 6 shows the atomic positions and excess spin density for the $Si_5O_{15}H_{12}$ cluster used to represent this state. The excited electron for the STE is located primarily on the

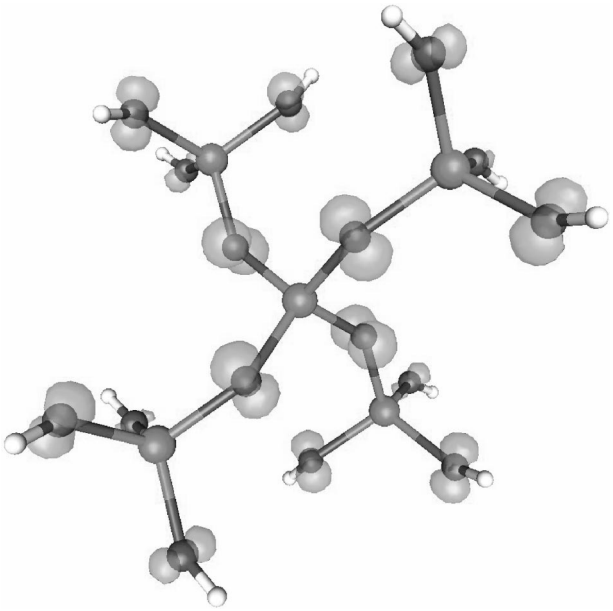

FIG. 5. A $Si_5O_{16}H_{12}$ cluster representing the perfect quartz configuration. An isosurface of the excess spin density of the triplet state calculated using DFT/B3LYP is shown. The excess spin density mainly resides on the O atoms, and is evenly distributed over the cluster, indicating a highly delocalized exciton.

central silicon atom of the cluster, and the hole is distributed over several oxygen atoms, as shown. The location of the excited electron and hole is correlated with an increase of negative charge on the silicon atom and an increase of positive charge on the oxygen atom. Results for singlet/triplet

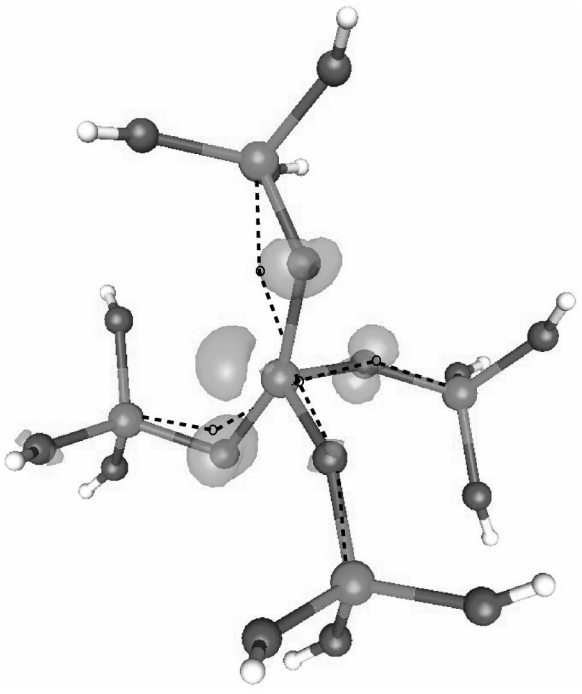

FIG. 6. A $Si_5O_{16}H_{12}$ cluster representing the STE-**B** STE. An isosurface of the excess spin density of the triplet state calculated using DFT/B3LYP is shown. The dashed lines indicate the positions of the atoms for the perfect crystal state. The excited electron of the STE is located primarily on the central silicon atom, while the hole is distributed over three oxygen atoms.

TABLE III. Luminescence (singlet/triplet splitting) of STE-**B** clusters. The basis sets used are the same as in Table II.

| Cluster size | Theory level | 6-31G* | 6-31G*+*s* | 6-31G*+*s*+*p* |
|---|---|---|---|---|
| $\mathbf{Si_2O_7H_6}$ | UHF | 4.38 | 4.35 | 4.58 |
| | UMP2 | 5.63 | 5.55 | 5.54 |
| | CCSD(T) | 3.92 | 4.79 | |
| | DFT-PW91 | 3.46 | 3.45 | 3.49 |
| | DFT-B3LYP | 3.92 | 3.94 | 3.99 |
| $\mathbf{Si_5O_{16}H_{12}}$ | UHF | 4.45 | 4.45 | 4.39 |
| | UMP2 | 5.72 | | |
| | DFT-PW91 | 3.52 | 3.52 | 3.53 |
| | DFT-B3LYP | 4.14 | 4.11 | 4.11 |
| $\mathbf{Si_8O_{25}H_{18}}$ | UHF | 5.01 | 4.95 | |
| | DFT-PW91 | 3.68 | 3.61 | |
| | DFT-B3LYP | 4.29 | 4.25 | |

differences in clusters of the STE-**B** geometry are shown in Table III. Adding diffuse functions to the basis set has significantly less effect on the calculated luminescence energy, as compared to the effect on the singlet/triplet splitting in the perfect crystal. For the DFT methods, the luminescence energy may be considered converged with respect to basis set with the use of one *s* diffuse function. Singlet/triplet splitting energies calculated using PW91 functional are consistently smaller than for any of the other methods.

With increasing cluster size, the luminescence energy is consistently larger. While the $Si_8O_{25}H_{18}$ was the largest size cluster possible in this work, the increasing luminescence energy is an indication that the calculations are not quite converged with respect to cluster size. Inspection of the atomic displacements, however, shows that the majority of the distortion due to the STE is contained within the clusters used. Atoms not included in the cluster are displaced by less than 0.05 Å from the quartz lattice positions.

### *3. STE-A*

Figure 7 shows the atom positions and the location of the excess spin density for this STE, calculated by DFT/B3LYP, using the $Si_5O_{16}H_{18}$ cluster. There is one significantly displaced oxygen atom, with a silicon–oxygen bond distance of 2.3 Å.

Table IV shows the luminescence energies calculated for this structure with different levels of theory, and different cluster sizes. The emission energy calculated at the UHF level is 1.55 eV for the $Si_2O_7H_6$ cluster. Fisher, Hayes, and Stoneham obtained a value of 1.5–1.9 eV[1] for similar clusters, using the minimal STO-3G basis set. Use of larger clusters, larger basis sets, and more accurate methods results in larger luminescence energy. The luminescence energy found using the DFT methods is close to the experimentally observed STE luminescence of 2.8 eV.

The singlet/triplet splitting for this state is converged with respect to basis set with the use of one $s'$ diffuse function, and the excess spin density is well contained within the $Si_5O_{16}H_{12}$ cluster.

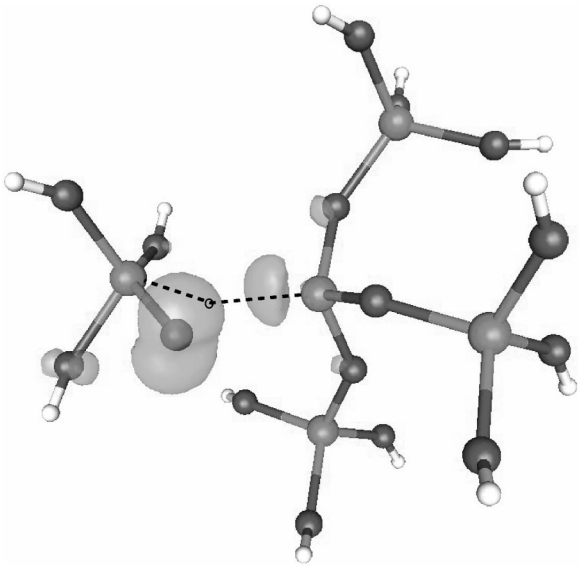

FIG. 7. A $Si_5O_{16}H_{12}$ cluster representing the STE-**A** STE. An isosurface of the excess spin density of the triplet state calculated using DFT/B3LYP is shown. The dashed lines indicate the positions of the atoms for the perfect crystal state. The excess spin density is localized at the broken bond, with the excited electron on the silicon atom, and the hole on the oxygen atom.

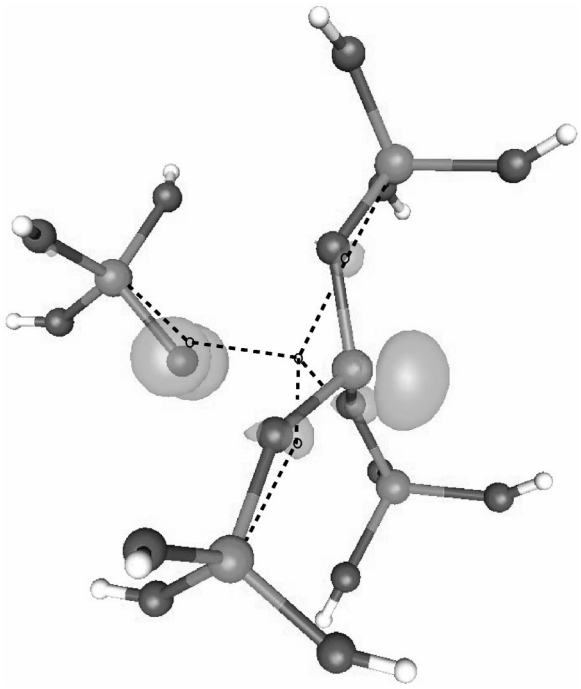

FIG. 8. A $Si_5O_{16}H_{12}$ cluster representing the Si-distorted configuration. An isosurface of the excess spin density of the triplet state calculated using DFT/B3LYP is shown. The dashed lines indicate the positions of the atoms for the perfect crystal state. The excess spin density, and therefore the STE, is localized at the broken bond, with the excited electron on the puckerd silicon atom, and the hole on the dangling oxygen atom.

#### *4. Silicon-distorted state*

Figure 8 shows the atomic positions and excess spin density for the $Si_5O_{15}H_{12}$ cluster used to represent this state. The singlet state of this structure has an open shell, and requires the use of a multireference wave function for a correct description. Results of UHF and UMP2 calculations for the singlet showed significant spin contamination, with $\langle S^2 \rangle$ in the range of 1.01. The value of $\langle S^2 \rangle = 1$ is typical for a low spin coupled diradical UHF calculation.

To obtain more adequate results, a CASSCF representation was used to calculate the singlet/triplet splitting for the **Si-dist** state. The CAS was constructed using the triplet state alpha corresponding orbitals as the initial orbitals. Both [2,2]- and [4,4]-CASSCF calculations were carried out, with the active space consisting of the highest occupied and lowest unoccupied molecular orbitals for the system. The multireference nature of the singlet state precluded the use of CCSD(T) to obtain a luminescence energy for this state. Despite being single determinant based methods, the DFT methods used in this work do not display any problem with spin contamination for this state.

None of the other STE states investigated in this work showed any significant spin contamination for any of the methods used. Additional CASSCF calculations of the STE-**A** state confirmed that the singlet state wave function does not have any significant multireference character, despite the relatively large Si–O separation.

The singlet/triplet splitting energy for the **Si-dist** state calculations are listed in Table V. CASSCF calculations performed using an active space of either [2,2] or [4,4] orbitals resulted in a neglible difference in the singlet/triplet splitting.

TABLE IV. Luminescence (singlet/triplet splitting) STE-**A** clusters. The basis sets used are the same as in Table II.

| Cluster size | Theory level | 6-31G* | 6-31G*+*s* |
|---|---|---|---|
| $\mathbf{Si_2O_7H_6}$ | UHF | | 1.55 |
| | CCSD(T) | | 3.10 |
| | DFT-PW91 | | 2.74 |
| | DFT-B3LYP | | 2.73 |
| $\mathbf{Si_5O_{16}H_{12}}$ | UHF | 1.55 | 1.64 |
| | UMP2 | 3.19 | |
| | DFT-PW91 | 2.66 | 2.79 |
| | DFT-B3LYP | 2.66 | 2.79 |
| DFT-plane wave | | 2.74 | |
| $\mathbf{Si_8O_{25}H_{18}}$ | UHF | 1.56 | 1.67 |
| | DFT-PW91 | 2.66 | 2.89 |
| | DFT-B3LYP | 2.66 | 2.90 |

TABLE V. Singlet/triplet energies for the silicon-distorted structure clusters. The basis sets used are the same as in Table II. Negative numbers for the luminescence energy indicate that the triplet state is lower than the singlet state for that cluster/method. This structure is at or near a crossing of the singlet and triplet surfaces.

| Cluster size | Theory level | 6-31G* | 6-31G*+*s* |
|---|---|---|---|
| $\mathbf{Si_2O_7H_6}$ | CAS-SCF | 0.00 | |
| | DFT-PW91 | −1.36 | |
| | DFT-B3LYP | −0.18 | |
| $\mathbf{Si_5O_{16}H_{12}}$ | CAS-SCF | 0.00 | 0.0 |
| | DFT-PW91 | −0.70 | −0.61 |
| | DFT-B3LYP | −0.33 | −0.27 |
| $\mathbf{Si_8O_{25}H_{18}}$ | DFT-PW91 | | 0.91 |
| | DFT-B3LYP | | 0.53 |

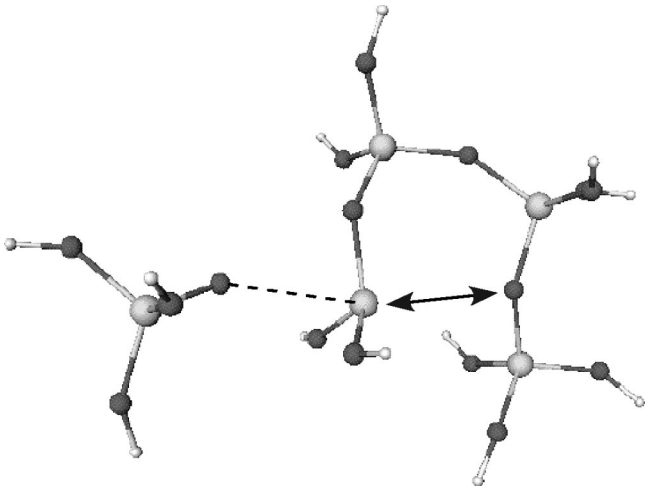

FIG. 9. An alternate structure for the Si-dist state was constructed to test for back-bonding of the puckered silicon atom to another network oxygen atom. The back-bonding was found to be unimportant.

Calculations using the B3LYP functional consistently yielded a singlet/triplet splitting energy closer to zero than calculations using the PW91 functional. Note that the value for the largest cluster calculated with the PW91 functional has converged to the supercell plane-wave result. Since the singlet/triplet splitting for this state is small or zero, the system is at or near a crossing of the singlet and triplet state surfaces, and the return to the singlet ground state would be via a nonradiative transition.

The possibility that the **Si-dist** state might be stabilized by back-bonding with another oxygen in the lattice, as seen with the oxygen vacancy,[29] was tested by contructing an alternate cluster in which the distance between the puckered silicon atom and the network oxygen is relatively close (2.5 Å), as shown in Fig. 9. The proximity to a back oxygen did not stabilize the **Si-dist** state. An alternative **Si-dist** state was found in the supercell system that differs in orientation such that the puckered silicon atom is pushed into a channel of the crystal instead of towards a network oxygen. The two **Si-dist** states have the same energy, to within 0.005 eV, indicating that the network oxygen has little effect on the energy of these states.

### B. Exciton localization

The difference between the crystal and both of the STE-O states was quantified by determining the localization of the excess spin density. The spatial extent of the excess spin density gives the effective size of the exciton. Localization is conveniently quantified by the participation function defined by

$$P = 1 + \sum_{i}^{N_{\text{atm}}} \left( \frac{w_i}{N_{\text{elec}}} \right)^2, \tag{1}$$

where $w_i$ is the spin population summed onto each atom, and $N_{\text{elec}}$ is the number of electrons in the state of interest. The number of electrons is set to 2 when analyzing excess spin density, and 1 when analyzing the localization of the excited electron and hole separately (since then the sum is over only one unpaired electron). The *inverse participation ratio* $P_{\text{inv}}$ is given by the inverse of Eq. (1). The effective center of the excess spin density is given by

$$\mathbf{R}_{\text{eff}} = \sum \frac{w_i}{N_{\text{elec}}} \mathbf{r}_i, \tag{2}$$

where $\mathbf{r}_i$ is a position vector for each atom, measured from a common reference point. The effective localization length, which is a measure of the spatial extent of the exciton, can then be calculated as

$$L_{\text{eff}} = \sum_{i}^{N_{\text{atm}}} \frac{w_i}{N_{\text{elec}}} |\mathbf{R}_{\text{eff}} - \mathbf{r}_i|. \tag{3}$$

For comparison, the effective spatial extent of the cluster itself is also calculated

$$L_{\text{eff}}^{\text{system}} = \sum_{i}^{N_{\text{atm}}} \left| \frac{\mathbf{r}_i}{N_{\text{atm}}} - \mathbf{r}_i \right|, \tag{4}$$

to determine how the cluster size affects the spatial extent of the exciton. For a fully delocalized state, $P = 1 + (1/N_{\text{atm}})$, or 1 in the limit as $N \to \infty$, $P_{\text{inv}} = 1$, and $L_{\text{eff}} = L_{\text{eff}}^{\text{system}}$. For a localized state, $P = 2$, $P_{\text{inv}} = 0.5$, and $L_{\text{eff}} = 0$.

The spin population for all the clusters was determined by the Mulliken analysis. The spin population of the smaller clusters was also analyzed using natural bond orbital (NBO) analysis.[30] The same basis set and level of theory were used for both analysis. For the small clusters, the difference in localization determined by the NBO and Mulliken analysis was small. Populations based on the NBO analysis were used for the separate examination of the hole and the electron, as described below.

Spin density localization in the perfect crystal for different cluster size and theoretical methods is shown in Table VI. The spin population is based on Mulliken analysis, using the 6-31G*+1*s* basis set. In general, the spin, and therefore the exciton, is more delocalized for calculations using the PW91 functional, less delocalized for the UHF calculations, and intermediate for B3LYP functional. Examination of these data shows that the spatial extent of the exciton increases as the size of the cluster increases. The size of the exciton is consistently quite similar to the total size of the cluster, illustrating that the exciton tends to delocalize over all the available volume in these clusters (see Fig. 5). (Figures 5–8 are available in color on EPAPS.[40])

Spin density localization for the STE-**B** state for different cluster size and theoretical methods is shown in Table VI. The larger value for $L_{\text{system}}^{\text{eff}}$, the measure of the effective size of the cluster, as compared to the perfect crystal clusters, illustrates that there is some outward displacement of the outermost atoms, as compared to their positions in the perfect crystal state. This is an indication that lattice relaxation is important, and even the largest clusters do not fully capture this effect. The effective size of the STE increases with cluster size, and is not fully converged for the largest cluster size. This is fully consistent with previous calculations investigating localization of the Al hole center in quartz.[31–33]

Comparison of spin density localization for the STE-**A** state for different cluster size and theoretical methods is

TABLE VI. Comparison of the localization of the spin density in the perfect quartz crystal (PQ), STE-A, and STE-B for different cluster size and theoretical methods. The participation ratio ($P_i$), inverse participation ratio ($P_i^{\text{inv}}$), and the effective localization length ($L_i^{\text{eff}}$), are shown. The results are based on the Mulliken analysis using the 6-31G*+1*s* basis set.

| Cluster size | $P_i$ PQ, STE-**B**, STE-**A** | $P_i^{\text{inv}}$ PQ, STE-**B**, STE-**A** | $L_i^{\text{eff}}$ (Å) PQ, STE-**B**, STE-**A** |
|---|---|---|---|
| $\mathbf{Si_2O_7H_6}$ | $\mathbf{L}_{\text{system}}^{\text{eff}}$=2.51, 2.51, 2.54 Å | | |
| UHF | 1.51, 1.44, 1.46 | 0.66, 0.69, 0.69 | 0.79, 0.92, 1.15 |
| DFT-PW91 | 1.23, 1.29, 1.34 | 0.81, 0.78, 0.75 | 1.90, 1.17, 1.32 |
| DFT-B3LYP | 1.22, 1.29, 1.38 | 0.82, 0.78, 0.73 | 1.80, 1.14, 1.26 |
| $\mathbf{Si_5O_{16}H_{12}}$ | $\mathbf{L}_{\text{system}}^{\text{eff}}$=3.56, 3.57, 3.56 Å | | |
| UHF | 1.37, 1.41, 1.48 | 0.73, 0.71, 0.67 | 2.24, 0.98, 1.13 |
| DFT-PW91 | 1.22, 1.21, 1.34 | 0.82, 0.83, 0.75 | 3.69, 1.52, 1.38 |
| DFT-B3LYP | 1.19, 1.24, 1.38 | 0.84, 0.81, 0.72 | 3.43, 1.35, 1.29 |
| $\mathbf{Si_8O_{25}H_{18}}$ | $\mathbf{L}_{\text{system}}^{\text{eff}}$=4.18, 4.23, 4.18 Å | | |
| UHF | 1.28, 1.32, 1.49 | 0.78, 0.75, 0.67 | 2.31, 1.10, 1.12 |
| DFT-PW91 | 1.14, 1.16, 1.34 | 0.88, 0.86, 0.75 | 4.15, 1.81, 1.42 |
| DFT-B3LYP | 1.12, 1.21, 1.39 | 0.89, 0.82, 0.72 | 3.95, 1.46, 1.30 |

shown in Table VI. The results show that the state is well contained in the $Si_5O_{16}H_{12}$ cluster. Comparison of the localization of the STE-**B** and STE-**A** shows that the number of atoms involved, as indicated by the participation ratio, in the STE-**A** state is fewer, yet the effective size of the STE is comparable, or in the case of the UHF calculations, sometimes even larger. This discrepancy is due to the distance between the atoms involved. In the case of STE-**B**, all of the involved atoms are still bound, with bond lengths less than 1.9 Å, while the STE-**A** is localized on two atoms that are not bonded, and separated by 2.5 Å. The difference in localization as calculated using PW91 and B3LYP is smaller for this state than for the STE-**B** state. Inclusion of exact Hartree–Fock exchange is important for a proper description of unpaired electrons.[34]

The separation of the excess spin density into a hole and excited electron can be defined by the change in atomic charge between the singlet and triplet state in the following way:

$$C_n^T - C_n^S = \Delta C_n, \tag{5}$$

where $C_n^T$ is the charge of atom $n$ in the triplet state, and $C_n^S$ is the charge of atom $n$ in the singlet state. The excited electron located at the atoms where $\Delta C_n$ is negative relative to the singlet, and the hole is located where $\Delta C_n$ is positive relative to the singlet.

The localization of the hole and excited electron, as determined by Eq. (5), for the STE-**B** state $Si_5O_{16}H_{12}$ clusters for different theoretical methods is shown in Table VII. The analysis is based on NBO analysis, using the 6-31G*+1*s* basis set. The difference in localization obtained by the different computational methods appears to be larger for the hole than for the excited electron. This implies that the localization of the exciton, as calculated here, is dominated by the characteristics of the hole. As for the localization of the STE as a whole, the degree of delocalization is greatest for DFT using the PW91 functional, smallest for UHF, and intermediate for B3LYP calculations.

### C. Luminescence lifetime

Since the STE involves a spin-forbiden transition, the lifetime of the luminescence can be estimated by calculating the transition dipole moment due to the spin–orbit coupling. The interacting states methods was employed as implemented in MOLPRO, where the transition moment reduces to just a weighted sum of dipole moments and spin-allowed transition dipole moments[35]

$$\langle S_0|\mu|T_1\rangle = \sum_i c_{iT_1}^* c_{iS_0} \langle i|\mu|i\rangle + \sum_i \sum_{j\neq i} c_{iT_1}^* c_{jS_0} \langle i|\mu|j\rangle, \tag{6}$$

where the spin–orbit coupled states are expanded with coefficients $c_{iS_0}$ and $c_{iT_1}$ in a basis of $S^2$ eigenfunctions. Calculations were performed with different numbers of singlet and triplet states included in the sum, ranging from one triplet and two singlet states, to eight singlet and eight triplet states. Two different basis sets were used: $cc-pVDZ$, and $cc-pVDZ-sp$, where the $sp$ functions are the $s$ and $p$ diffuse functions used in the aug-cc-pVDZ basis set. All the spin–orbit calculations used state-averaged CASSCF orbitals. Due to computational limitations, lifetimes were calcu-

TABLE VII. Comparison of localization of the hole and excited electron for the STE-**B** state $Si_5O_{16}H_{12}$ cluster for different theoretical methods. Symbols are defined as in Table VI. The analysis is based on NBO analysis, using the 6-31G*+1*s* basis set.

| Method | $P_i$ | $P_i^{\text{inv}}$ | $L_i^{\text{eff}}$ (Å) |
|---|---|---|---|
| **Hole** | | | |
| UHF | 1.80 | 0.56 | 0.32 |
| DFT-PW91 | 1.14 | 0.87 | 2.00 |
| DFT-B3LYP | 1.20 | 0.83 | 1.78 |
| **Electron** | | | |
| UHF | 1.48 | 0.67 | 0.74 |
| DFT-PW91 | 1.34 | 0.74 | 1.04 |
| DFT-B3LYP | 1.39 | 0.72 | 0.85 |

TABLE VIII. Predicted luminescence lifetime for STE-**B** and STE-**A**, based on spin–orbit coupling calculations of the transition dipole for the $Si_2O_7H_6$ clusters.

| **STE-B** States ($S/T$) | Lifetime, ms cc-pVDZ | cc-pVDZ+$sp$ |
|---|---|---|
| 2/1 | 2.68 | 2.95 |
| 4/2 | 0.09 | 0.31 |
| 6/2 | 0.24 | 0.35 |
| 8/2 | 0.44 | 0.55 |
| 6/4 | 0.47 | 0.30 |
| 8/4 | 0.47 | 0.31 |
| 8/8 | 0.51 | 0.33 |
| **STE-A** States ($S/T$) | | |
| 2/1 | 2.91 | 2.92 |
| 4/2 | 5.76 | 3.56 |
| 6/2 | 3.17 | 3.28 |
| 8/2 | 2.88 | 3.28 |
| 6/4 | 2.43 | 2.73 |
| 8/4 | 2.44 | 2.64 |
| 8/8 | 2.40 | 2.61 |

lated using only the smallest constructed clusters. As shown in Table VIII, the estimated luminescence lifetime is sensitive to both the basis set and the number of states included in the sum. The luminescence lifetime for STE-**A** is estimated to be 3 ms. For STE-**B** the luminescence lifetime is estimated to be 0.3 ms. The lifetime for STE-**B** is more sensitive to the basis set than for STE-**A**. It has been shown that the clusters used for these calculations are not large enough to fully capture the properties of the STE-**B** state.

### D. Cluster geometry relaxation

It is informative to examine the results of structural relaxations of the STE states using different electronic structure methods, and different environments (cluster versus supercell). Relaxation of atomic coordinates is also used to test the stability of the STE configurations in clusters.

Figure 10 shows the results of relaxing the STE-**A** state in a cluster, using UHF. The stretched silicon–oxygen distance increased from 2.3 to 2.5 Å. Further relaxation using B3LYP resulted in negligible change in the structure.

When the Si-dist geometry was relaxed at the UHF level, the broken silicon–oxygen bond distance stretched further, from 2.54 to 2.81 Å. Figure 11 shows the atom positions before and after relaxation. The Si-dist is stable in a supercell and in clusters of this size.

Relaxation of STE-**B** in a cluster environment resulted in a structure very similar to the Si-dist state. The silicon atom that is nearly in the plane of three of its neighboring oxygen atoms passes through the plane during the relaxation, into a puckered configuration. There is a broken bond, with a silicon–oxygen distance length of 2.80 Å. The energy converged to a value only 0.02 eV different than that of the STE-Si relaxed structure. The structures cannot reach an identical minimum because the terminal atoms are frozen. Figure 12 shows the placement of the atoms before and after relaxation. Several attempts were made to find the STE-**B** structure in a cluster environment, using clusters up to $Si_8O_{25}H_{18}$, without success. Calculations using exact exchange (UHF or B3LYP) resulted in either an STE-**A** or Si-dist state. Calculations using PW91 resulted in a fully delocalized state, with the excess spin density spread around the edge of the cluster, possibly due to edge effects caused by the termination of the cluster with OH groups.

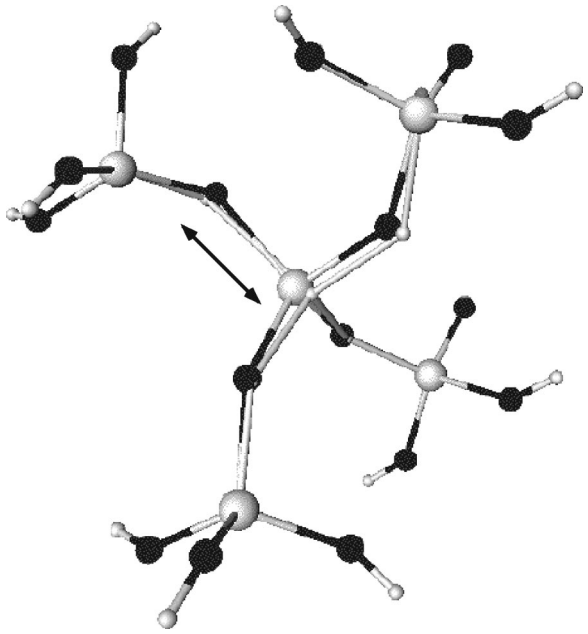

FIG. 10. Relaxation of the PW91 optimized STE-**A** cluster using UHF leads to very little structural change. The oxygen and silicon atom move slightly further apart, as shown by the arrow, to a distance of 2.5 Å, from 2.3 Å. The final structure is represented by the thinner, light gray framework superimposed on the starting structure.

As shown by both the luminescence energy and the participation ratio data, the clusters used are clearly not large

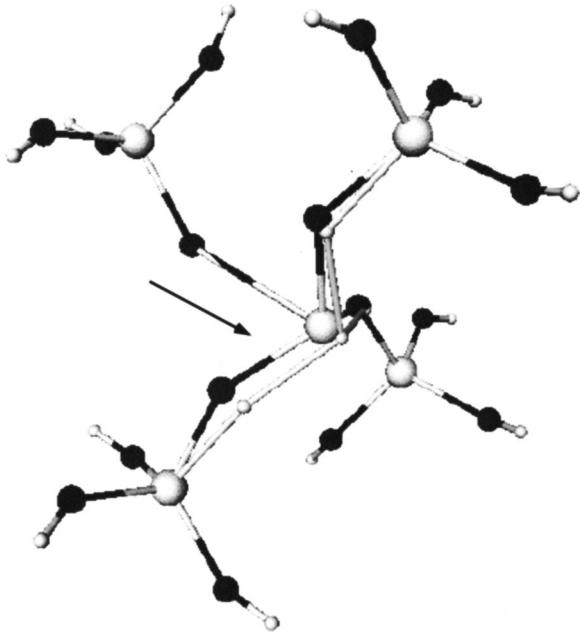

FIG. 11. Relaxation of the Si-dist cluster using UHF results in an increase in the Si–O distance. The structure is qualitatively the same.

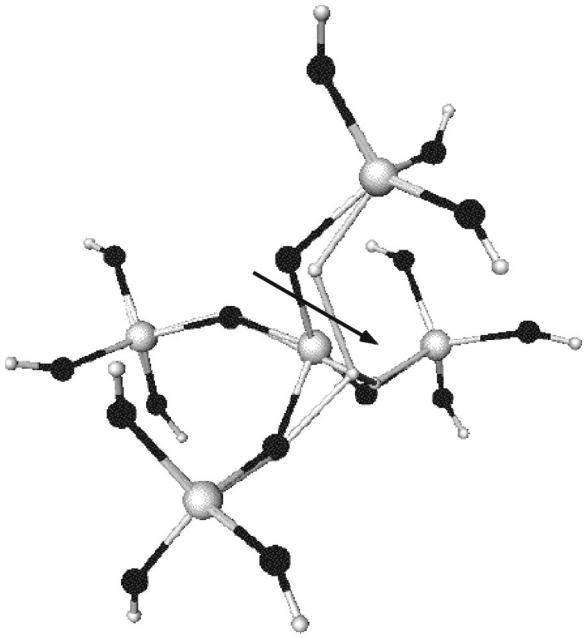

FIG. 12. Relaxation of the STE-**B** cluster using UHF results in a structure that is qualitatively different than the initial structure. The silicon atom relaxes to a puckered position, breaking one bond, and moving through the plane of the three other attached oxygen atoms, as indicated by the arrow. The final structure is similar to the Si-distorted state. The final structure is represented by the thinner, light gray framework superimposed on the starting structure.

enough to fully capture the STE-**B** state. Small perturbations can lead to large changes in atomic coordinates since the triplet state energy surface is quite flat.

### E. Effect of localization on the singlet–triplet splitting

It is known that there is error in the relative energies calculated using DFT/PW91, when comparing localized and delocalized states.[36] The tendency is for DFT/PW91 to favor delocalized states. The energy of delocalized states is artificially lowered due to the approximate nature of the PW91 functional. An analogous effect has been noted in calculations of a hole at an Al substitutional impurity in quartz, where a delocalized hole was found using PW91, while experimental results indicate a localized hole. The hole is, however,[31,32] calculated to be localized in UHF, i.e., when exact exchange is included (free of self-interaction).[34] This contradiction may be used to rule out the delocalized structure for the hole.

In the case of the STE in quartz, however, it is not possible to rule out the partially delocalized state, STE-**B**. The calculated luminescence energy is in the range of the experimentally observed luminescence at about 4 eV that has multiple sources. There is one source with characteristics consistent with the presence of an intrinsic STE such that the luminescence decreases in intensity as defects are generated by irradiation.[37]

An examination of the data for the singlet/triplet splitting energies, and the inverse participation ratio, $P_{inv}$, for the different geometries, shows that there is a trend in the size of the underestimation of the energy of the triplet state. Since the cluster tests show that B3LYP gives more accurate results, this trend can be quantified by comparing the singlet/triplet splitting energy as calculated using PW91 and B3LYP. The difference in the splittings, defined by

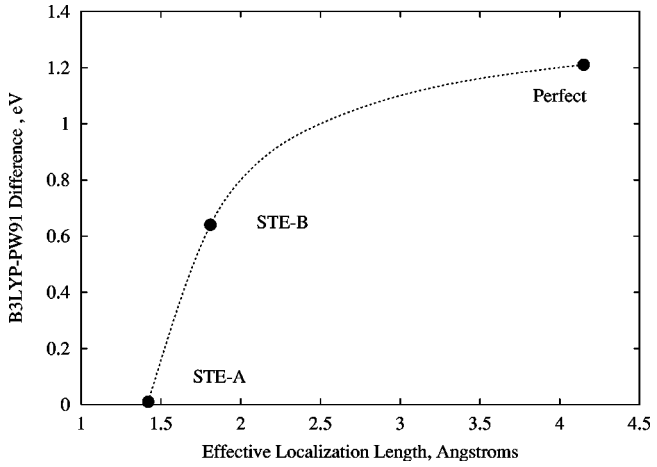


FIG. 13. The relationship between $L_{eff}$ and the difference in the singlet–triplet splitting calculated using B3LYP and PW91—an estimate of the error in the PW91 calculation.

$$\text{B3LYP}-\text{PW91}=(T^{\text{B3LYP}}-S^{\text{B3LYP}})-(T^{\text{PW91}}-S^{\text{PW91}}), \quad (7)$$

gives a value for the error in the triplet state energy calculated without exact exchange. This value can then be compared to the inverse participation ratio to obtain an estimated correction based on the delocalization of the state in question.

Figure 13 shows the trend in the B3LYP-PW91 difference with the PW91 effective localization length, $L_{eff}$, as calculated for the $Si_8O_{25}H_{18}$ clusters. For the STE-**A** state, the STE is very localized, and the B3LYP-PW91 difference is close to zero. As the exciton becomes more delocalized, the error increases, and then levels off to around 1.2 eV for the fully delocalized crystal state exciton.

This trend could be used to estimate the accuracy of the singlet/triplet difference when it is not possible to use methods that include exact exchange, and to make an estimated correction to the triplet state energy. Note that additional confirmation would be needed for states which require a multireference wave function. For the Si-dist state, the correction as formulated above would actually be negative. This is consistent with the CASSCF results. It appears that the B3LYP calculations may improve the description of these types of states as well, since the singlet/triplet splitting for these states is likely smaller (closer to zero) than the difference obtained using PW91. It does not appear possible, however, to relate this negative correction to the localization of the state.

## IV. CONCLUSIONS

In this work, we have studied the energetics and structures of three different STE structures for quartz, which were predicted by plane-wave DFT calculations. The STE-Si state has been found to be stable in cluster calculations using UHF, and in a supercell calculation using plane-wave DFT.

This structure is very near a curve crossing of the triplet and singlet surfaces, and may, therefore, correspond to a nonradiative transition to the ground state. The STE-**B** structure, with a calculated luminescence energy of 4–5 eV, has been shown to be unstable in a $Si_5O_{16}H_{12}$ cluster at the UHF level, possibly because of its delocalized nature. Relaxation of this STE-**B** structure in the cluster geometry leads to the STE-Si structure. Luminescence from this structure may be a component of the broad luminescence band observed at 4.0 eV.[37] The STE-**A** structure has a calculated luminescence energy of 2–3 eV. It is stable in a cluster, using the various theoretical methods that include exact exchange (UHF, B3LYP), but in PW91 supercell calculations it only corresponds to a nearly flat plateau on the potential energy surface. Relaxation in the supercell using PW91 results in a structure related to the STE-**B** structure, which is 0.5 eV lower in energy. This situation is likely due to the tendency of DFT methods without exact exchange to favor delocalization of unpaired electrons (and holes) because of the self-interaction.

The optimized structure of the STEs in clusters is different depending on the initial displacement of the atoms in the center of the cluster. If one oxygen atom is displaced, the STE-**A** structure is obtained. If the displacement corresponds to the positions of the STE-**B**, with three displaced oxygen atoms, or the STE-Si, with a displaced silicon atom, the result is the STE-Si structure. Differences between supercell and cluster results remain unresolved. Further investigation of this problem requires methods that treat correlation and exchange in supercell or extended systems such as those using embedded methods.[38,39]

There is a definite trend in the apparent error in the PW91 calculations with respect to the inverse participation ratio of the exciton. More delocalized states have greater error, meaning that the energy of the triplet state is decreased by a greater amount. This trend could possibly be used to formulate a correction to the energy of the triplet state as calculated with PW91.

## ACKNOWLEDGMENTS

R.M.V. would like to thank the Environmental Molecular Science Laboratory at Pacific Northwest National Laboratory for the hospitality during her tenure. We would like to acknowledge support of R.M.V., K.A.P., and L.R.C. by the Division of Chemical Sciences, Office of Basic Energy Sciences, Department of Energy, and of R.M.V. and H.J. by the Division of Materials Sciences and Engineering, Office of Basic Energy Science, Department of Energy. Part of this research was performed and the calculations carried out at the University of Washington. Part of this research was performed in the William R. Wiley Environmental Molecular Sciences Laboratory, a national scientific user facility sponsored by the Department of Energy, Office of Biological and Environmental Research located at Pacific Northwest National Laboratory. Battelle operates the Pacific Northwest National Laboratory for the Department of Energy.

[1] A. J. Fisher, W. Hayes, and A. M. Stoneham, J. Phys.: Condens. Matter **2**, 6707 (1990).
[2] I. N. Levine, *Physical Chemistry* (McGraw-Hill, New York, 1978).
[3] J. Song, L. R. Corrales, G. Kresse, and H. Jónsson, Phys. Rev. B **64**, 134102 (2001).
[4] W. J. Weber, R. C. Ewing, C. R. A. Catlow *et al.*, J. Mater. Res. **13**, 1434 (1998).
[5] K. Tanimura, T. Tanaka, and N. Itoh, Phys. Rev. Lett. **51**, 423 (1983).
[6] S. Guizard, P. D'Oliveira, P. Daguzan, P. Martin, P. Meynadier, and G. Petite, Nucl. Instrum. Methods Phys. Res. B **116**, 43 (1996).
[7] S. Guizard, P. Martin, G. Petite, P. D'Oliveira, and P. Meynadier, J. Phys.: Condens. Matter **8**, 1281 (1996).
[8] C. Itoh, K. Tanimura, N. Itoh, and M. Itoh, Phys. Rev. B **39**, 11183 (1989).
[9] G. Pacchioni and G. Ierano, Phys. Rev. Lett. **79**, 753 (1997).
[10] M. Cannas. M. Barbara, R. Boscaine, A. Collura, F. M. Galard, and S. Varisco, J. Non-Cryst. Solids **245**, 190 (1999).
[11] P. J. Alonso, L. E. Halliburton, E. E. Kohnke, and R. B. Bossoli, J. Appl. Phys. **54**, 5369 (1983).
[12] K. Tanimura and L. E. Halliburton, Phys. Rev. B **34**, 2933 (1986).
[13] A. N. Trukhin, J. Non-Cryst. Solids **189**, 1 (1995).
[14] W. Hayes, M. J. Kane, O. Salminen, R. L. Wood, and S. P. Doherty, J. Phys. C **17**, 2943 (1984).
[15] C. Itoh, K. Tanimura, and N. Itoh, J. Phys. C **21**, 4693 (1988).
[16] M. A. Stevens-Kalceff and M. R. Phillips, Phys. Rev. B **52**, 3122 (1995).
[17] M. Georgiev and N. Itoh, J. Phys.: Condens. Matter **2**, 10021 (1990).
[18] G. Pacchioni and G. Ierano, Phys. Rev. B **57**, 818 (1998).
[19] J. Song, H. Jónsson, and L. R. Corrales, Nucl. Instrum. Methods Phys. Res. B **166–167**, 451 (2000).
[20] A. Smith, J. K. Wiggs, H. Jónsson, L. R. Corrales, P. Nachtigall, and K. D. Jordan, J. Chem. Phys. **102**, 1044 (1995).
[21] M. J. Frisch, G. W. Trucks, H. B. Schlegel *et al.*, GAUSSIAN 98, Revision A1, Gaussian Inc., Pittsburgh, PA, 1998.
[22] M. Dupuis, A. Marquez, and E. R. Davidson, HONDO 99 (1999), based on HONDO 95.3, M. Dupuis, A. Marquez, and E. R. Davidson, Quantum Chemistry Program Exchange (QCPE) Indiana University, Bloomington, IN 47405.
[23] H.-J. Werner and P. Knowles, MOLPRO *is a package of ab initio programs* (2002), with contributions from J. Almlf, R. D. Amos, A. Berning *et al.*
[24] J. Song, R. M. Van Ginhoven, L. R. Corrales, and H. Jónsson, Faraday Discuss. **117**, 303 (2000).
[25] F. Sim, C. R. A. Catlow, M. Dupuis, and J. D. Watts, J. Chem. Phys. **95**, 4215 (1991).
[26] G. Pacchioni and G. Ierano, Phys. Rev. B **56**, 7304 (1997).
[27] A. H. Edwards, Phys. Rev. Lett. **71**, 3190 (1993).
[28] J. Sauer, P. Ugliengo, E. Garronen, and V. R. Saunders, Chem. Rev. **94**, 2095 (1994).
[29] J. Song, L. R. Corrales, and H. Jónsson, Mater. Res. Soc. Symp. Proc. **540**, 379 (1999).
[30] NBO version 3.1, E. D. Glendening, A. E. Reed, J. E. Carpenter, and F. Weinhold.
[31] A. Continenza and A. D. Pomponio, Phys. Rev. B **54**, 13687 (1996).
[32] M. Magagnini, P. Giannozzi, and A. D. Corso, Phys. Rev. B **61**, 2621 (2000).
[33] J. Laegsgaard and K. Stokbro, Phys. Rev. B **61**, 12590 (2000).
[34] G. Pacchioni, F. Frigoli, D. Ricci, and J. A. Weil, Phys. Rev. B **63**, 054102 (2000).
[35] B. Hess, C. M. Marian, and S. Peyerimhoff, in *Modern Electronic Structure Theory, Part 1*, edited by D. Yarkony (World Scientific, Singapore, 1995), Vol. 2, p. 152.
[36] V. Perebeinos, P. B. Allen, and M. Weinert, Phys. Rev. B **62**, 12589 (2000).
[37] A. Corazza, B. Crivelli, M. Martini, G. Spinolo, and A. Vedda, Phys. Rev. B **53**, 9739 (1996).
[38] D. Erbetta, D. Ricci, and G. Pacchioni, J. Chem. Phys. **113**, 10744 (2000).
[39] D. Ricci, G. Pacchioni, M. A. Szymanski, A. L. Shluger, and A. M. Stoneham, Phys. Rev. B **64**, 224101 (2001).
[40] See EPAPS Document No. E-JCPSA6-118-707314 for color figures 5 through 8. A direct link to this document may be found in the online article's HTML reference section. The document may also be reached via the EPAPS homepage (http://www.aip.org/pubservs/epaps.html) or from ftp.aip.org in the directory /epaps/. See the EPAPS homepage for more information.